

## C<sub>60</sub> thin film growth on graphite: Coexistence of spherical and fractal-dendritic islands

Hui Liu and Petra Reinke<sup>a)</sup>

*Department of Materials Science and Engineering, University of Virginia, Charlottesville, Virginia 22904-4145*

(Received 4 January 2006; accepted 16 February 2006; published online 26 April 2006)

The initial growth stage of C<sub>60</sub> thin film on graphite substrate has been investigated by scanning tunneling microscopy in ultrahigh vacuum at room temperature. The C<sub>60</sub> layer grows in a quasi-layer-by-layer mode and forms round, monolayer high islands on the graphite surface. The islands are confined by terraces on the graphite surface and the mobility of C<sub>60</sub> fullerenes across steps is low in all layers. The second and all subsequent layers adopt a fractal-dendritic shape, which was confirmed by calculating the fractal dimension ( $D=1.74$  prior to island coalescence) and is in agreement with a diffusion limited aggregation. The profound differences between the growth of C<sub>60</sub> layers on graphite (first layer) and on C<sub>60</sub> surfaces (second and higher layers) are caused by the restriction of the C<sub>60</sub> mobility on the highly corrugated fullerene surfaces. The orientation of the fractal islands follows the hexagonal symmetry of the densely packed (111) surface of the fullerene lattice, which introduces a bias in the direction of molecule movement. The differences in surface topography on the nanoscale determine the mode of film growth in this van der Waals bonded system. © 2006 American Institute of Physics. [DOI: [10.1063/1.2186310](https://doi.org/10.1063/1.2186310)]

### INTRODUCTION

Fullerenes and, in particular, C<sub>60</sub> have received much attention because of their unique structural,<sup>1</sup> chemical,<sup>2,3</sup> and electronic properties.<sup>4,5</sup> Many studies focus on applications in nanotechnology,<sup>6</sup> the interaction of fullerenes with different surfaces,<sup>7-10</sup> and recently the potential of fullerenes as a material for solar cells<sup>11</sup> was realized. To further explore the use of fullerenes in nanotechnology applications, our knowledge at a fundamental level how fullerene molecules interact physically and electronically with each other and with their local environment must be extended.

In our present study we selected a purely van der Waals bonded system and studied the interaction of C<sub>60</sub> with the surface of highly oriented pyrolytic graphite (HOPG). The HOPG-fullerene interface presents a weakly interacting system and charge transfer to the fullerene molecules is absent.<sup>10</sup> The bonding strength between graphite-C<sub>60</sub> molecules and C<sub>60</sub>-C<sub>60</sub> is very similar,<sup>10,12,13</sup> which allows us to isolate the influence of surface structure and nanotopography on the fullerene layer growth as it progresses beyond the first monolayer. Previous investigations of the adsorption of C<sub>60</sub> on graphite<sup>7,12,14-20</sup> remained inconclusive, yielding a wide range of observed growth modes, and a concise description and understanding of the growth process is still missing. In this letter, we report the observation of a mixed growth mode of C<sub>60</sub> on HOPG at room temperature, in which an island and fractal-dendritic growth occur simultaneously. A qualitative model is developed to describe the coexistence of the different growth modes, which is linked to the influence of surface topography on the growth kinetics and diffusion processes at the surface.

### EXPERIMENT

The experiments were performed in an Omicron variable temperature ultrahigh vacuum scanning probe microscope (UHV-SPM) system that consists of a preparation chamber and a scanning tunneling microscope (STM) chamber. The sample is transferred between the chambers without breaking the vacuum. Atomically flat HOPG surfaces were obtained by cleavage in air at room temperature, and subsequent annealing at 300 °C for at least 10 h. The C<sub>60</sub> powder was sublimed from a tantalum crucible at a pressure below  $1 \times 10^{-9}$  mbar (chamber base pressure of  $3 \times 10^{-10}$  mbars). The deposition experiments were carried out in a cumulative manner and STM images were recorded after each deposition event. Cumulative deposition durations were 35 s [0.52 monolayer (ML)], 50 s (0.86 ML), and 110 s (1.72 ML), respectively, at a deposition rate of 0.0155 ML/s. The stability of the graphite surface and the C<sub>60</sub> overlayer structure was sufficient to perform the experiment in this sequential manner. Degradation and significant changes in the surface structure are observed after more than 2 days. STM tips were mechanically cut Pt/Ir wires. All STM images were acquired in the constant current mode at room temperature and are displayed such that the scan lines are horizontal and scanning proceeds from the bottom to the top.

Before the deposition of C<sub>60</sub>, the HOPG substrate is flat and step edges of HOPG can be resolved clearly. After the deposition, STM imaging of C<sub>60</sub> on HOPG is carried out with a sample bias voltage of more than 1.2 V to engage the fullerene states in the tunneling process, and the image remained unchanged for higher bias voltage. Lower bias voltage, which can be used to image the underlying graphite surface, causes the probing tip to “machine” the C<sub>60</sub> films

<sup>a)</sup>Electronic mail: [pr6e@virginia.edu](mailto:pr6e@virginia.edu)

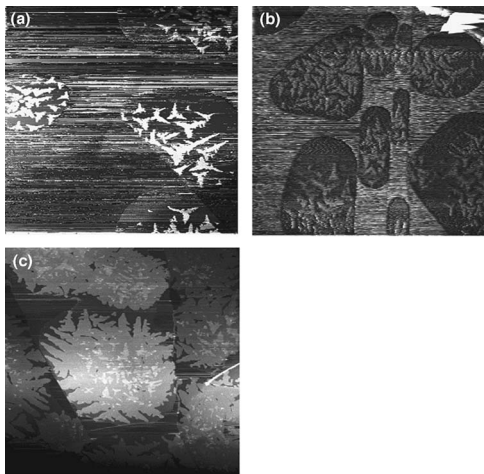


FIG. 1. This figure shows the characteristic features of the  $C_{60}$  film on a preannealed HOPG substrate at different cumulative deposition times. (a) Cumulative deposition time is 35 s and area is  $2000 \times 2000 \text{ nm}^2$ . (b) Cumulative deposition time is 50 s and area is  $3000 \times 3000 \text{ nm}^2$ . (c) Cumulative deposition time is 110 s and area is  $3000 \times 3000 \text{ nm}^2$ . Tunneling conditions were 1.2 V and 0.1 nA. The underlying graphite substrate exhibits large terraces with mostly single atom layer step height and straight edges.

rather than image them. With a bias voltage of 0.5 V, the tip moves through the film, breaks it, and removes most  $C_{60}$  molecules from the scanned area. The graphite atomic structure cannot be imaged with atomic resolution using the tunneling conditions required to image  $C_{60}$  molecules, which prevents simultaneous imaging of both lattices.

We observed in the large majority of images the appearance of streaks, which is caused by tip-induced movement and/or the presence of highly mobile fullerene molecules [two-dimensional (2D) molecule gas] on the surface.<sup>21–23</sup> Streaks are mostly observed on the bare graphite surface and rarely on top of  $C_{60}$  islands, which can in turn be used to distinguish these two surfaces. A saw-tooth-like STM tunneling current characteristic prevails in streaky areas and indicates the dominance of tip induced molecule movement or trapping of molecules in the tip-surface gap. Reduction of the tunneling current to values below 0.1 nA is insufficient to prevent this effect on graphite, and no changes in the imaging of the pure fullerene surfaces are observed. It is predicted<sup>13,24</sup> that the average energy barrier of displacement of  $C_{60}$  on the bare graphite surface is much smaller than that of  $C_{60}$  on the  $C_{60}(111)$  surface, which facilitates molecule displacement by the tip and favors the formation of a 2D molecule gas on graphite.

## RESULTS AND DISCUSSION

Figures 1(a)–1(c) illustrate the progression of  $C_{60}$  film growth on the HOPG substrate at different cumulative deposition times. From Fig. 1 it can be seen that differently shaped  $C_{60}$  islands are present at all times. The first layer of  $C_{60}$  film grows in round, elongated islands which are confined to the terraces defined by the graphite substrate; on top of these islands, small fractal-dendritic shaped islands are observed (a discussion of the fractal dimension follows in the next paragraphs). The straight graphite step edges (which are

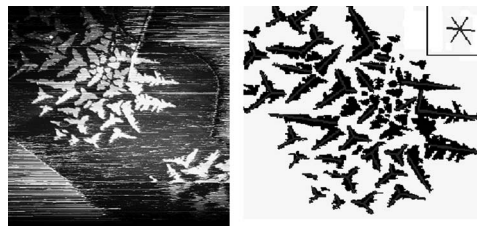


FIG. 2. Image of the second layer of an STM image recorded after 35 s deposition time [see Fig. 1(a)]. This image was extracted from the STM image to isolate the characteristic fractal-dendritic shape of the second-layer islands. The original figure is shown on the left hand side, and the extracted image, which includes solely the second layer, is located on the right hand side. Straight lines were drawn to indicate their orientation and the insert at upper right side is included as a guidance to identify the preferred island orientations.

commonly observed on clean graphite surfaces) are still discernible and clearly provide a barrier to fullerene diffusion on the graphite surface, which leads to confinement of first-layer islands on the terraces. The curved boundaries of the islands, however, are not related to underlying graphite terrace steps but evolve due to the adoption of the thermodynamically most stable shape of the island. Second-layer islands are located at the central part of first-layer islands, the same holds true for third layer islands, which are located in the center part of the second layer. A constant distance between the boundaries of upper layer islands to lower layer island edges is observed. In the last image the appearance of the first small islands of an additional layer can be seen and the  $n+1$  layer islands begin to form before the  $n$  layer is completed. This is most easily seen in the growth of fractal islands on the round first-layer islands. The  $C_{60}$  molecules, which land on an island, are confined by the island edges due to the Ehrlich-Schwoebel barrier, which prevents a downward diffusion.  $C_{60}$  molecules are therefore confined to a single layer and cannot contribute to growth on the lower lying island. First-layer and second-layer islands increase in size as the deposition time increases, [shown in Fig. 1(b)] at roughly equivalent rates.

In the first layer elliptically shaped, relatively large islands dominate, except in those cases, where growth is restricted by confinement on terraces. This suggests that lateral growth dominates even for longer deposition times in the first layer. In addition, it is noted that static coalescence in the first layer occurred when the size of neighboring islands increases in the course of deposition. After the longest deposition time of 110 s, shown in Fig. 1(c), second-layer islands begin to coalesce, but the shape of their boundaries still reflects the original fractal-dendritic shapes. The third and fourth layers, also in the fractal-dendritic shape, begin to nucleate on the top of the second layer.

In Fig. 2, only the second layer islands, which were extracted from a STM image [see Fig. 1(a)], are shown. This image is used to illustrate the characteristic fractal-dendritic shape and the triangular symmetry. Images of this type are used in the determination of the fractal dimension for each layer and island type. Three kinds of island shapes can be identified: small size compact irregular shapes, middle-size

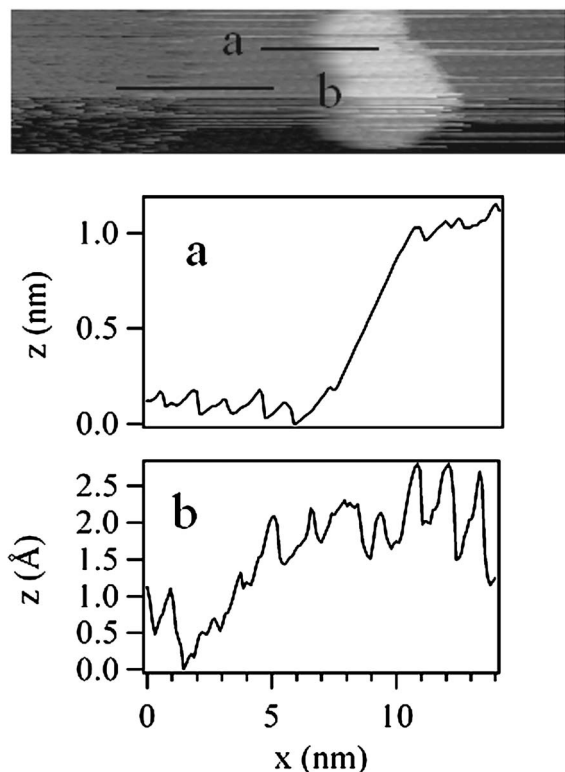


FIG. 3. (a) High magnification STM topography image, which shows the edge of a first-layer island on HOPG and a second-layer island with atomic resolution. (b) Line profile along the line indicated by the arrow in image (a).

triangular shapes, and large-size dendritic shapes. Larger, well-defined islands are usually surrounded by some smaller, more compact islands, which indicates a competition for mobile fullerene molecules during growth and a local depletion of growth species. Moreover, it is noted that second-layer islands are characterized by a preferred direction of orientation in six directions, which is commensurate with the hexagonal symmetry of the underlying C<sub>60</sub> (111) plane (see Fig. 3) and a consequent directional bias of the diffusion processes on the surface.

Figure 3 is a high magnification STM topography image, which shows the edge of a first-layer island on HOPG and a second-layer island. The C<sub>60</sub> molecules are arranged in a hexagonal close-packed structure, corresponding to the densely packed C<sub>60</sub> (111) plane, which was confirmed by the hexagonal symmetry in fast Fourier transformation. The apparent step height of the first-layer island is only about 0.2 nm, which is considerably smaller than the C<sub>60</sub> diameter (1 nm). The height of the second-layer island is about 1 nm, which reflects the diameter of the molecule. The reason for this exceptionally low apparent height of the first layer is unclear: electronic effects leading to a deviation of the apparent height from the molecule diameter have been observed on metal surfaces<sup>8,9,25</sup> but seem unlikely in the absence of charge transfer or chemisorption, and the reason for the reduced apparent height remains unclear at present. However, it can be concluded from these data, that the first island layer is most likely not thicker than one monolayer of C<sub>60</sub> molecules. The observation of different growth modes supports this conclusion.

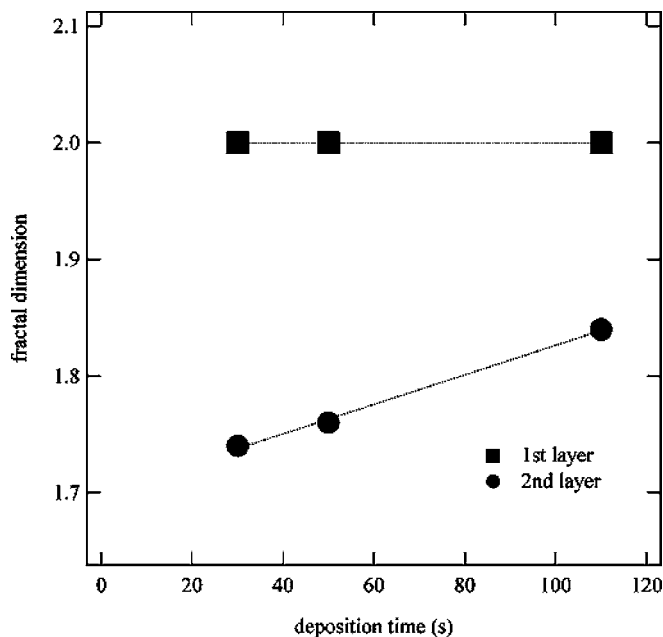


FIG. 4. Development of the fractal dimension as a function of cumulative deposition time. The broken line is added as guidance for the eyes and results from a line fit of the data points.

A comparison to other experimental results from the literature<sup>7,12,14-20</sup> remains problematic due to the diverse deposition conditions and substrate pretreatments, which were used. We observed that the substrate cleanliness has a profound effect on the growth of C<sub>60</sub> layers on graphite. Reproducibility of the growth mode and fractal shapes can only be achieved if a prolonged substrate annealing is introduced. Without this critical sample preparation step a wide variety of intermediate shapes, with a varying degree of fractal and round island characteristics and an average height often commensurate with a double-layer thickness of the islands, could be observed. The strong influence of even small amounts of residual impurities on the growth mode is likely the reason for the considerable differences in the experiments described in the literature.

In order to quantify the observations described in the previous paragraph we performed an analysis of the fractal dimensions of the islands by digitizing the patterns into a black-white mode by means of Scion image analysis software. The box-counting method<sup>26</sup> was used to characterize the dimension of the islands and the results are summarized in Fig. 4. To obtain the fractal dimensions the patterns for the respective layers were divided into squares with various sides  $A$  and the occupied pixels were counted. The occupation number scaled as  $N$  ( $\ln N \propto \ln D$ ), where  $D$  is the fractal dimension. The shapes have a fractal dimension in between 1 and 2, where a fractal dimension of 2 characterizes a round island. Figure 4 illustrates the development of the fractal dimension with deposition time. The dimension value of roundish first-layer islands is always 2 independent of deposition time, and corresponds to the Euclidean dimension of the object. For the second-layer islands an average dimension of 1.74 is measured and commensurate with the fractal-dendritic shape of the second layer. The dimension value of the second-layer island increases with deposition time and

reflects the “closure” of the branched regions. The third-layer islands have a lower dimension value (1.55) since the islands are somewhat fragmented as they are observed at the onset of growth.

The formation of dendritic islands can be described by the diffusion-limited aggregation (DLA), a computer simulation framework in which particles undergoing random walk stick to the surface of a growing aggregate whenever they encounter it. The growing branches block the attachment of the next molecules and therefore the lengthening of branches is favored over the occupation of energetically preferable adsorption sites. Only the ability of the molecules to detach and reattach to the island boundary makes it possible to minimize the length of the boundary and reach a thermodynamically stable, roundish shape with a minimized length of the boundary line. The preferential orientation of the dendritic islands with respect to the underlying first-layer fullerene lattice stems from anisotropy of the  $C_{60}$  diffusion determined by the lattice symmetry. Attachment and reattachment of  $C_{60}$  to the growing island are biased by the directional diffusion, and certain growth directions will therefore be favored, which is clearly seen in Fig. 2.

The observed structures can be compared to the DLA-like patterns described by Wynblatt *et al.*,<sup>27</sup> who developed a modified DLA mode, which differed from conventional DLA in that site-specific sticking coefficients were allowed to differ from unity. Our experimental STM images are in good agreement with their simulated results when the sticking probability was reduced to the range of 0.02–0.05, while sticking probabilities at higher coordination sites were held at unity.

Combined with previous discussion in the present paper, we suggest that the early growth stage of  $C_{60}$  on HOPG at room temperature takes place through two-dimensional island coalescence and predominantly in a quasi-layer-by-layer manner.  $C_{60}$ – $C_{60}$  bonds in the film are of the van der Waals type, and the bond strength of  $C_{60}$  to graphite is only slightly different.<sup>10,12,13,25,28,29</sup> The adsorption energies of  $C_{60}$  on graphite surface and  $C_{60}(111)$  surface were calculated by Gravil *et al.*<sup>13</sup> to be 968 and 813 meV. These values are supported by thermal desorption experiments, which yield a slightly higher temperature for  $C_{60}$  desorption from graphite<sup>13</sup> than from  $C_{60}$ . The room temperature diffusion barriers, however, differ significantly and values of 13 meV ( $C_{60}$  on graphite) and 168 meV [ $C_{60}$  on  $C_{60}(111)$ , averaged over all directions] are obtained.<sup>13</sup> Molecules on graphite should therefore be highly mobile at room temperature, which is commensurate with our observations.

We suggest that the profound difference in first- and second-layer growth modes originates from the significant differences in the diffusion energies rather than the relatively small changes in bonding energies. The energy required for the detachment of  $C_{60}$  molecules from island boundaries is comparable for both surfaces, but the ability of the molecule to subsequently move to a favorable bonding site is severely restricted on the  $C_{60}$  surface. The strong directional dependence of the diffusion on the fullerene surface is clearly reflected in the shape of second and higher number islands. The ability of  $C_{60}$  to easily move on the graphite surface

leads to the formation of the thermodynamically favored shape of round islands with a minimal boundary length, while this process is kinetically hindered on fullerene surfaces.

## CONCLUSIONS

In conclusion, we have performed deposition of  $C_{60}$  on the surface of HOPG at room temperature to explore the initial stages of  $C_{60}$  thin films growth. It is confirmed that the first layer of  $C_{60}$  is a monolayer and we conclude that the growth mechanism of the initial stage is two-dimensional island coalescence and predominantly in a quasi-layer-by-layer manner. The fractal-dendritic nature of the second and all subsequent layers was confirmed by calculating the fractal dimension ( $D=1.74$  prior to island coalescence). Our experimental results for  $C_{60}$  island formation on  $C_{60}$  are in agreement with growth through a diffusion limited aggregation. The profound differences between the growth of  $C_{60}$  layers on graphite and on  $C_{60}$  surfaces are caused by the restriction of the  $C_{60}$  mobility on the highly corrugated fullerene surfaces. The differences in surface topography on the nanoscale determine the mode of film growth. Future experiments will explore the low coverage regime for first-layer growth, and the high coverage regime, where the formation of additional fractal layers will be investigated. We aim to develop a concise DLA description and to determine the critical values of the system (diffusion constants, energy barriers at step edges, and layer intermixing).

## ACKNOWLEDGMENTS

This work was supported by the MRSEC Center for Nanoscopic Materials Design sponsored by the National Science Foundation and the start-up funding from the University of Virginia (P.R.).

- <sup>1</sup>K. Tanigaki, I. Hirose, T. Ebbesen, J. Mizuki, and J. Tsai, *J. Phys. Chem. Solids* **54**, 1645 (1993).
- <sup>2</sup>P. Fagan, J. Calabrese, and B. Malone, *Science* **252**, 1160 (1991).
- <sup>3</sup>J. Shih, Y. Chao, M. Sung, G. Gau, and C. Chiou, *Sens. Actuators B* **76**, 347 (2001).
- <sup>4</sup>J. Weaver, J. Martins, T. Komeda, Y. Chen, T. R. Ohno, G. Kroll, N. Troullier, E. Haufler, and R. Smalley, *Phys. Rev. Lett.* **66**, 1741 (1991).
- <sup>5</sup>J. L. Martins, N. Troullier, and J. H. Weaver, *Chem. Phys. Lett.* **180**, 457 (1991).
- <sup>6</sup>A. P. G. Robinson, R. E. Palmer, T. Tada, T. Kanayama, and J. A. Preece, *Appl. Phys. Lett.* **72**, 1302 (1998).
- <sup>7</sup>R. Lüthi, E. Meyer, H. Haefke, L. Howald, W. Gutmannsbauer, and H.-J. Güntherodt, *Science* **266**, 1979 (1994).
- <sup>8</sup>E. I. Altman and R. J. Colton, *Phys. Rev. B* **48**, 18244 (1993).
- <sup>9</sup>J. K. Gimzewski, S. Modesti, and R. R. Schlittler, *Phys. Rev. Lett.* **72**, 1036 (1994).
- <sup>10</sup>P. Reinke, H. Feldermann, and P. Oelhafen, *J. Chem. Phys.* **119**, 12547 (2003).
- <sup>11</sup>S. Licht, O. Khaselev, P. A. Ramakrishnan, D. Faiman, E. A. Katz, A. Shames, and S. Goren, *Sol. Energy Mater. Sol. Cells* **51**, 9 (1998).
- <sup>12</sup>M. F. Luo, Z. Y. Li, and W. Allison, *Surf. Sci.* **402–404**, 437 (1998).
- <sup>13</sup>P. A. Gravil, M. Devel, Ph. Lambin, and X. Bouju, *Phys. Rev. B* **53**, 1622 (1996).
- <sup>14</sup>M. R. C. Hunt and R. E. Palmer, *Surf. Rev. Lett.* **3**, 937 (1996).
- <sup>15</sup>H. Yu, J. Yan, Y. Li, W. S. Yang, Z. Gu, and Y. Wu, *Surf. Sci.* **286**, 116 (1993).
- <sup>16</sup>S. Suto, A. Kasuya, C. Hu, A. Wawro, T. Goto, and Y. Nishina, *Surf. Rev. Lett.* **3**, 927 (1996).
- <sup>17</sup>S. Suto, A. Kasuya, C. Hu, A. Wawro, K. Sakamoto, T. Goto, and Y.

- Nishina, *Thin Solid Films* **281–282**, 602 (1996).
- <sup>18</sup> S. Szuba, R. Czajka, A. Kasuya, A. Waweo, and H. Rafii-Tabar, *Appl. Surf. Sci.* **144–145**, 648 (1999).
- <sup>19</sup> D. J. Kenny and R. E. Palmer, *Surf. Sci.* **447**, 126 (2000).
- <sup>20</sup> S. Okita and K. Miura, *Nano Lett.* **1–2**, 101 (2001).
- <sup>21</sup> M. Böhringer, W.-D. Schneider, and R. Berndt, *Surf. Sci.* **408**, 72 (1998).
- <sup>22</sup> S. Berner, M. Brunner, L. Ramoino, H. Suzuki, and H.-J. Güntherrodt, *Chem. Phys. Lett.* **348**, 175 (2001).
- <sup>23</sup> L. Bartels, G. Meyerm, and K. H. Rieder, *Phys. Rev. Lett.* **79**, 697 (1997).
- <sup>24</sup> J. G. Kushmerick and P. S. Weiss, *J. Phys. Chem. B* **102**, 10094 (1998).
- <sup>25</sup> C. Rey, J. García-Rodeja, and L. J. Gallego, *Phys. Rev. B* **55**, 7190 (1997).
- <sup>26</sup> L. Niemeyer, L. Pietronero, and H. J. Wiesmann, *Phys. Rev. Lett.* **52**, 1033 (1986).
- <sup>27</sup> P. Wynblatt, J. J. Metosi, and J. C. Heyraud, *J. Cryst. Growth* **102**, 618 (1990).
- <sup>28</sup> L. A. Girifalco, M. Hodak, and R. S. Lee, *Phys. Rev. B* **62**, 13104 (2000).
- <sup>29</sup> L. A. Girifalco and M. Hodak, *Phys. Rev. B* **65**, 125404 (2002).